SPEKTRA: Jurnal Fisika dan Aplikasinya
Volume 10, Issue 2, August 2025
Homepage: doi.org/10.21009/SPEKTRA

DOI: doi.org/10.21009/SPEKTRA.102.01

Theoretical Study of Positron-Electron Scattering with Thermal-Volkov Wavefunction

Narayan KC[1], Suresh Prasad Gupta[1], Kishroi Yadav[1], Saddam Husain Dhobi[2,*]

[1]*Department of Physics, Patan Multiple Campus, Tribhuvan University, Lalitpur 44700, Nepal*
[2]*Central Department of Physics, Tribhuvan University, Kirtipur 44618, Nepal*

*Corresponding Author Email: saddam@ran.edu.np

Received: 12 May 2025
Revised: 5 June 2025
Accepted: 10 June 2025
Online: 15 August 2025
Published: 31 August 2025

SPEKTRA: Jurnal Fisika dan Aplikasinya
p-ISSN: 2541-3384
e-ISSN: 2541-3392

ABSTRACT

This study investigates the differential cross-section (DCS) for laser-assisted positron-electron scattering in a Gaussian wave packet, within a linearly polarized laser field in a thermal environment. For this, a theoretical model was developed with a designed thermal Gaussian Volkov wavefunction, vector potential, and scattering matrix with the application of the Bessel function. The developed model was computed using the Matlab programming language to study the nature of the developed model of DCS. The observation shows that the DCS initially increases with positron energy, reaching a peak around 0.5 eV; after that, it decreases with further increases in energy and approaches a constant at high energies. This is due to changing dynamics of positron-electron interactions with resonance occurring at specific energies. Also, the observation shows that temperature plays a significant role, especially at lower energies, with higher temperatures (325 K) enhancing the DCS due to increased thermal excitation of the target electrons. The study also explores the influence of the z-value and found that higher z-values lead to a decrease in the DCS due to the Coulombic interaction becoming stronger. Moreover, the effects of external factors such as the number of laser field photons and pulse duration are considered. The observation shows that shorter laser pulse durations and higher photon energies enhance the scattering process, while longer pulse durations result in a decrease in DCS. This study aids in optimizing technologies like PET imaging, plasma diagnostics, and particle accelerators by revealing how positron-electron scattering varies with energy, temperature, and laser parameters. It supports real-world applications in medical, space, and materials science.

Keywords: differential cross section, positron energy, temperature, z-value, laser field photons, pulse duration, scattering, resonance, thermal effects

INTRODUCTION

Scattering refers to the process where particles or waves interact with each other or a medium, causing a change in direction or energy. This concept dates back to J.J. Thomson's discovery of the electron in 1897, which helped extend physics beyond classical theories. Rutherford's elastic scattering experiment in 1911 led to the discovery of the atomic nucleus. Scattering can occur through electromagnetic interactions, such as photon scattering, and is valuable in fields like physics, chemistry, material science, and remote sensing [1]. Scattering processes are categorized into elastic and inelastic scattering. Elastic scattering conserves total energy, while inelastic scattering involves energy exchange between particles. Scattering theory helps in understanding the interactions of particles through both classical and quantum frameworks. Classical scattering deals with macroscopic particles and uses principles like Newton's laws, while quantum scattering analyzes subatomic particles through advanced techniques like the Schrödinger equation and Feynman diagrams [2]. The electron, discovered in 1897, is a fundamental particle with a negative charge and plays a key role in atomic structure and chemistry. Its counterpart, the positron, was discovered in 1932 and has applications in medical imaging. Laser-assisted scattering involves laser fields that influence particle interactions, leading to energy shifts and new interaction channels.

Bound states refer to systems where particles are confined within a region due to attractive forces, like electrons bound to atomic nuclei. Volkov wave functions describe quantum states of charged particles in external electromagnetic fields, essential for understanding laser-matter interactions. Reduced dimensionality models simplify complex systems, aiding in the study of particle interactions, while positron Gaussian wave packets provide insights into positron-laser dynamics [3]. Positron-electron scattering with thermal-Volkov wavefunctions involves the application of Volkov states, which are solutions to the Dirac equation in the presence of electromagnetic fields. These states are crucial for understanding scattering processes, particularly in strong-field quantum electrodynamics (QED). The integration of thermal effects into these Volkov states describes the behavior of charged particles in external electromagnetic fields, which is essential for analyzing scattering events in QED [4]. Recent advancements have led to generalized Volkov solutions that accommodate multimode laser fields, enhancing the applicability of these states in various scattering scenarios [5]. Incorporating thermal effects into Volkov states allows for the modeling of positron scattering at thermal energies, which is critical for understanding interactions with atomic and molecular targets. Research has shown that modified effective range theory can accurately predict elastic cross-sections for positron scattering from various targets, including noble gases [6].

The Volkov solutions can be modified to account for electron states in plasma environments, which differ significantly from vacuum conditions. This adaptation is vital for understanding scattering in complex media [7]. While the focus on Volkov states provides a robust

framework for analyzing scattering processes, it is essential to consider the limitations and assumptions inherent in these models, particularly when applied to non-ideal conditions such as high-density plasmas or complex molecular interactions. Positron-atom collisions, especially in the presence of a laser field, have gained significant attention in both practical applications and fundamental research. The ionization processes, in particular, have been extensively studied. Theoretical investigations of positron-impact ionization of hydrogen atoms under laser fields have been explored using the Dirac–Volkov formalism, extending the nonrelativistic Schrödinger approach to relativistic treatments. These studies calculate triple differential cross-sections to understand the influence of the laser field on the scattering process [8].

Positron and electron interactions with atomic systems differ significantly. While electron scattering theories were initially developed and later adapted to positrons, positrons interact differently with targets due to the absence of exchange effects [9]. At higher energies, positrons may form positronium or excite and ionize the target atom. In contrast, at low energies, positrons typically undergo elastic scattering. Positron scattering plays a crucial role in understanding matter structure and has applications ranging from astrophysical research to medical imaging. Key phenomena during positron collisions include annihilation (at low energies) and positronium formation, the latter being a central challenge in theoretical models [10]. The positron-hydrogen system, one of the simplest three-particle systems, has been the subject of ongoing theoretical and experimental studies. Research on positronium formation cross-sections has been limited due to the difficulty in generating high-intensity positron beams [11]. Furthermore, studies by Dhobi et al. [12] have shown that the differential cross-section for inelastic scattering increases when the target absorbs energy from a laser field, with maxima observed at specific energy emission points, further complicating the scattering process.

The resonant laser-assisted annihilation and production of electron-positron pairs have been theoretically investigated by Roshchupkin et al. [13]. Under specific resonant conditions—namely, a narrow angle between initial particle momenta and energy excess over a threshold—the second-order quantum electrodynamics process reduces to two first-order processes: laser-assisted annihilation and production via a real intermediate photon. The resonant differential cross-section obtained can significantly exceed the conventional Bhabha scattering cross-section in the absence of an external field. Pan et al. [14] examined the ionization of atomic hydrogen by fast positrons in an external, linearly polarized laser field, focusing on small momentum transfers. The fast positron's continuum states were described using Volkov wave functions, and the ejected electron using a Coulomb–Volkov approach. Despite the high laser intensities, only weak dressing of the target atom was assumed, allowing use of time-dependent perturbation theory. Du et al. [15] studied positron-muon scattering under laser fields using the first Born approximation. Their findings revealed multiple nonlinear effects, including multiphoton interactions, angular oscillations, dark windows, and asymmetries in angular distributions. The total differential cross-section was found to decrease with increasing incident positron energy. Bornikov et al. [16] analyzed Compton decay of positronium by twisted (Bessel) photons. Interestingly, most unique features of the twisted photons were lost

due to averaging over the azimuthal angle, making the differential probability equivalent to that of a plane-wave photon with a specific propagation angle. In a separate advancement, Duo et al. [17] proposed a spin-polarized positron acceleration mechanism using electrostatic and transition radiation fields generated by an ultrarelativistic electron beam through multilayer microhole array films. This setup achieved high polarization (>90%) and acceleration gradients (~TeV/m), offering a novel pathway for compact positron accelerator development. However, despite these advancements, none of the above studies incorporated thermal effects in their theoretical treatment. The approach presented in the theoretical study of positron-electron scattering with thermal-Volkov wavefunctions uniquely addresses the impact of temperature on positron-electron interactions by incorporating thermal effects into the Volkov formalism, a gap not covered in the earlier referenced works.

The research gap in the field of laser-assisted positron-electron scattering lies in the limited understanding of how various factors, such as positron energy, temperature, target material properties, laser field intensity, and pulse duration, interact to influence the DCS in a thermal environment. While previous studies have explored positron scattering at individual parameters, there is a lack of comprehensive models that consider the combined effects of laser fields, thermal excitation, and material properties on DCS. Furthermore, the role of resonance phenomena and the influence of high Z-values in the scattering process remain underexplored. This study aims to fill these gaps by developing a novel model that incorporates a thermal Gaussian Volkov wavefunction and a vector potential to analyze the DCS in laser-assisted scattering experiments. The objective is to provide a detailed understanding of the complex dynamics between positrons and target electrons, particularly the effects of temperature, laser photon intensity, and pulse duration on scattering efficiency, with a focus on resonance interactions and the thermal environment. This research will offer valuable insights for optimizing experimental conditions and advancing the understanding of positron scattering in the presence of laser fields and thermal effects.

METHOD

System Setup

For considered of the system where the positron is the projectile particle and the electron is the target particle, the Hamiltonian of the system in one dimension, in the absence of laser fields, is given by [11]:

$$\mathrm{H} = \frac{1}{2}\mathrm{p}_1^2 + \frac{1}{2}\mathrm{p}_2^2 + \mathrm{V}(r_1) - \mathrm{V}(r_2) - \mathrm{V}(r_1 - r_2) \tag{1}$$

Here, $\mathrm{p}_1(\mathrm{p}_2)$ and $r_1(r_2)$ are, respectively, the momentum and position of the positron (electron) and $\mathrm{V}(r)$ is the soft-core Coulomb potential [18]:

$$\mathrm{V}(x) = \frac{1}{\sqrt{r^2 + a^2}} \tag{2}$$

Here, $a = \frac{\hbar^2}{mQ^2} = \frac{1}{Q^2}$, where Q is the potential strength parameter, m is mass, and $\hbar$ is plank constant. The evolution of the system is determined by solving the TDSE in two spatial degrees of freedom with respect to r:

$$i\frac{\partial}{\partial t}\psi(r,t) = \hat{H}\psi(r,t) \tag{3}$$

In EQUATION (3), $\hat{H}$ is the Hamiltonian operator and ψ is wave fucntion. The initial system wave function of the positron is expressed in [11] as:

$$\psi(r,t=0) = \frac{1}{(2\pi\sigma^2)^{1/4}} e^{\frac{(r-r_0)^2}{4\sigma^2}} e^{ip_0 r} \tag{4}$$

The positron wave function is represented by a Gaussian wave packet with momentum p_0 at $t = 0$, σ is the packet width with a typical choice of 30 a.u., r is the position which varies, and r_0 is the position when $t = 0$. Since the energies of the positron–hydrogen bound states are lower than the ground state energy of the H atom in the present reduced-dimensionality model, the formation of three-body bound states is energetically prohibited in the nonradiative scattering process. Application of a linearly polarized laser field with its polarization direction parallel to the initial momentum of the positron would significantly confine the motion of the electron and positron to the polarization direction [19]. Also, the Hamiltonian in the presence of a laser field for the considered system is expressed as:

$$H_L = H + V_L \tag{5}$$

where H is the laser-free atomic Hamiltonian given in EQUATION (1), and V_L represents the laser–atom interaction. The interaction between the laser field, the incident positron, and the target electron in the length gauge is expressed as:

$$V_L(r,t) = E(t)(r) \tag{6}$$

where the electric field E(t) is obtained from the vector potential A(t) using $\mathrm{E(t)} = -\frac{\mathrm{dA(t)}}{\mathrm{dt}}$ and $\mathrm{A(t)} = \mathrm{A_0} f(t)\cos[\omega(t - t_0) + \phi]$, where ω is the frequency of the photon, $\mathrm{A_0}$ is amplitude, t_0 is the initial time, ϕ is the phase [15-20], and $f(t)$ is defined as:

$$f(t) = \sin^2\left(\frac{\pi}{2}\frac{t}{\tau_R}\right), \qquad 0 < \mathrm{t} < \tau_R \tag{7}$$

where τ_R is the pulse duration time and t is time. Hence, the electric field $E(t)$ is obtained as:

$$E(t) = -A_0\left(\frac{\pi}{2\tau_R}\sin\left(\frac{t\pi}{\tau_R}\right)\cos[\omega(t-t_0)+\phi] - \omega\sin[\omega(t-t_0)+\phi]\sin^2\left(\frac{\pi}{2}\frac{t}{\tau_R}\right)\right) \tag{8}$$

Now, the laser–atom interaction potential is given as:

$$V_L = -r\cos\theta\left(A_0\left(\frac{\pi}{2\tau_R}\sin\left(\frac{t\pi}{\tau_R}\right)\cos[\omega(t-t_0)+\phi]\right.\right.$$
$$\left.\left.-\omega\sin[\omega(t-t_0)+\phi]\sin^2\left(\frac{\pi}{2}\frac{t}{\tau_R}\right)\right)\right) \quad (9)$$

The thermodynamic properties of thermal electrons in scattering events under a laser field were investigated. The results show that at low field amplitudes (0.1–0.9 a.u.), destructive interference occurs, while higher amplitudes (1–2.5 a.u.) show superposition and Coulomb potential-like behavior at 2.5–3 a.u. Thermodynamic energy is constant with temperature, except at 2.5 a.u., and the thermodynamic potential increases linearly above 3.5 a.u. with temperature [21]. The study investigates laser-assisted thermal electron-hydrogen atom elastic scattering using Volkov-Thermal wavefunctions. It considers electron energies from 0.511 to 4 MeV and laser photon energies between 1–3 eV at room temperature (280–300 K). Destructive interference occurs when a thermal electron absorbs a photon, but no interference is observed when emitting an electron.

Wavefunction Construction

The DCS for thermal electrons is found to be greater than for non-thermal electrons in the presence of the laser field [22]. Now, the positron wave function from EQUATION (4) in the laser field is obtained with the help of the electron being present in the laser field using the Volkov wave function. With superposition, we have for the positron, in atomic units,

$$X(r,t) = \frac{1}{(2\pi)^{3/2}}\frac{1}{(2\pi\sigma^2)^{\frac{1}{4}}}e^{\frac{(r-r_0)^2}{4\sigma^2}}e^{ipr}$$
$$\times\exp\left(i\boldsymbol{p}.\left\{\frac{[\sin(\omega t_0-\phi+\omega t)+\sin(\omega t_0-\phi)]}{\omega}\right\}\right.$$
$$\left.-\frac{1}{2}\left\{\frac{\left[\sin\left(\frac{\pi t}{\tau_R}+\omega t-\omega t_0+\phi\right)\right]}{\frac{\pi}{\tau_R}+\omega}+\frac{\left[\sin\left(\frac{\pi t}{\tau_R}-\omega t+\omega t_0-\phi\right)\right]}{\frac{\pi}{\tau_R}-\omega}\right\}\right) \quad (10)$$
$$\times\exp\left(-\frac{iEt}{\hbar}\right)-k_eT_e\exp(i\omega_{eT}t)$$

EQUATION (10) represents the thermal Volkov wave function for the positron, which extends the Gaussian wave packet defined in EQUATION (4). This means that when the positron is placed in both a laser and thermal environment, its wave function is described by the thermal Volkov wave function. The last term of EQUATION (10) represents the thermal contribution, where k_e denotes the thermal conductivity of the electron, T_e is the temperature of the system in which the electron is present, indicating a thermal electron, and ω_{eT} corresponds to the electron energy within the thermal environment.

Scattering Matric Formulation

Now, the scattering matrix is given by

$$S = \int_{\infty}^{\infty} dt \, \langle \mathrm{X_f(r,t)} | \, \mathrm{V_L}(r) | \mathrm{X_i(r,t)} \rangle \tag{11}$$

For spherical coordinates, the expansion of EQUATION (11) is expressed as EQUATION (12) with substituting the above values of the potential and wavefunction:

$$\begin{aligned} S = \frac{A_0}{(2\pi)^3 (2\pi\sigma^2)^{\frac{1}{2}}} \int_{\infty}^{\infty} dt \int_0^{2\pi} d\phi \int_0^{\pi} \sin\theta \; d\theta \int_0^{\infty} r^2 dr \Bigg[e^{\frac{(r-r_0)^2}{4\sigma^2}} e^{-ip_f r} \\ \times \exp\Bigg(-i\boldsymbol{p_f}. \Bigg\{ \frac{[\sin(\omega t_0 - \phi + \omega t) + \sin(\omega t_0 - \phi)]}{\omega} \Bigg\} \\ - \frac{1}{2} \Bigg\{ \frac{\left[\sin\left(\frac{\pi t}{\tau_R} + \omega t - \omega t_0 + \phi\right)\right]}{\frac{\pi}{\tau_R} + \omega} + \frac{\left[\sin\left(\frac{\pi t}{\tau_R} - \omega t + \omega t_0 - \phi\right)\right]}{\frac{\pi}{\tau_R} - \omega} \Bigg\} \Bigg) \\ \times \exp\left(+ \frac{iE_f t}{\hbar} \right) - k_e T_{ef} \exp(-i\omega_{eTf} t) \Bigg] r \cos\theta \Bigg\{ \omega \sin^2\left(\frac{\pi t}{\tau_R}\right) \sin[\omega(t - t_0) + \phi] \\ - \frac{\pi}{\tau_R} \sin\left(\frac{\pi t}{\tau_R}\right) \cos[\omega(t - t_0) + \phi] \Bigg\} \Bigg[e^{\frac{(r-r_0)^2}{4\sigma^2}} e^{ip_i r} \\ \times \exp\Bigg(i\boldsymbol{p_i}. \Bigg\{ \frac{[\sin(\omega t_0 - \phi + \omega t) + \sin(\omega t_0 - \phi)]}{\omega} \Bigg\} \\ - \frac{1}{2} \Bigg\{ \frac{\left[\sin\left(\frac{\pi t}{\tau_R} + \omega t - \omega t_0 + \phi\right)\right]}{\frac{\pi}{\tau_R} + \omega} + \frac{\left[\sin\left(\frac{\pi t}{\tau_R} - \omega t + \omega t_0 - \phi\right)\right]}{\frac{\pi}{\tau_R} - \omega} \Bigg\} \Bigg) \\ \times \exp\left(- \frac{iE_i t}{\hbar} \right) - k_e T_{ei} \exp(i\omega_{eTi} t) \Bigg] \end{aligned} \tag{12}$$

$$S = \frac{A_0}{(2\pi)^3(2\pi\sigma^2)^{\frac{1}{2}}}\int_{\infty}^{\infty} dt \int_0^{2\pi} d\phi \int_0^{\pi} \sin\theta\cos\theta\, d\theta \int_0^{\infty} r^3 dr \left[\left[e^{\frac{(r-r_0)^4}{4\sigma^2}} e^{ip_i r - ip_f r}\right.\right.$$
$$\times \exp\left(\left(-ip_f + ip_i\right)\cos\theta\left\{\frac{\sin(c_2+\omega t)+\sin(c_2)}{\omega}\right\}\right.$$
$$\left.-\frac{1}{2}\left\{\frac{\sin(a_1 t + c_1)}{a_1} + \frac{\sin(b_1 t + c_2)}{b_1}\right\}\right)\exp\left(-iE_i t + iE_f t\right)$$
$$- k_e T_{ei}\exp(i\omega_{eTi}t)\left\{e^{\frac{(r-r_0)^2}{4\sigma^2}} e^{-ip_f r}\exp\left(-ip_f\cos\theta\left\{\frac{\sin(c_2+\omega t)+\sin(c_2)}{\omega}\right\}\right.\right.$$
$$\left.\left.-\frac{1}{2}\left\{\frac{\sin(a_1 t + c_1)}{a_1} + \frac{\sin(b_1 t + c_2)}{b_1}\right\}\right)\exp\left(iE_f t\right)\right\}\Bigg] \quad (13)$$
$$-\left[k_e T_{ef}\exp\left(-i\omega_{eTf}t\right)e^{\frac{(r-r_0)^2}{4\sigma^2}} e^{ip_i r}\exp\left(ip_i\cos\theta\left\{\frac{\sin(c_2+\omega t)+\sin(c_2)}{\omega}\right\}\right.\right.$$
$$\left.\left.-\frac{1}{2}\left\{\frac{\sin(a_1 t + c_1)}{a_1} + \frac{\sin(b_1 t + c_2)}{b_1}\right\}\right)\right]\Bigg]\left\{\omega\sin^2\left(\frac{\pi t}{\tau_R}\right)\sin[\omega t + c_1]\right.$$
$$\left.-\frac{\pi}{\tau_R}\sin\left(\frac{\pi t}{\tau_R}\right)\cos[\omega t + c_1]\right\}$$

Assuming $\pi/\tau_R + \omega = a_1$ and $\pi/\tau_R - \omega = b_1$, $-\omega t_0 + \phi = c_1$, $\omega t_0 - \phi = c_2$ and $z = \left\{\frac{\sin(c_2+\omega t)+\sin(c_2)}{\omega}\right\} - \frac{1}{2}\left\{\frac{\sin(a_1 t + c_1)}{a_1} + \frac{\sin(b_1 t + c_2)}{b_1}\right\}$, solving, we get from EQUATION (13),

$$S = \frac{A_0}{(2\pi)^3(2\pi\sigma^2)^{\frac{1}{2}}}\left[(A_1 - A_2) - [A_3 - A_4]\right]\left\{\omega\sin^2\left(\frac{\pi t}{\tau_R}\right)\sin[\omega t + c_1]\right.$$
$$\left.-\frac{\pi}{\tau_R}\sin\left(\frac{\pi t}{\tau_R}\right)\cos[\omega t + c_1]\right\} \quad (14)$$

$\Delta p = p_f - p_i$, $\Delta E = \frac{\pi}{\tau_R} + \omega$. We have, only taking the angular real part and applying Bessel function. More details of A_1, A_2, A_3 and A_4 are in appendix:

$$A_1 = \frac{\pi}{4}\sum_{n=-\infty}^{\infty} i^n J_n(\Delta p z)\left[\pi\omega sin(c_1) + \frac{\pi^2}{2\tau_R} sin\,(c_1)\right]\left[\frac{1 - e^{i(n+2)\pi}}{n+2}\right.$$
$$\left.-\frac{1 - e^{i(n-2)\pi}}{n+2}\right]\frac{n!\, e^{i\Delta p r_0}}{(-i\Delta p)^{n+1}} \quad (15)$$

$$A_2 = \frac{\pi k_e T_{ei}}{4}\sum_{n=-\infty}^{\infty} i^n J_n(p_f z)\left[\pi\omega sin(c_1) + \frac{\pi^2}{2\tau_R} sin\,(c_1)\right]\left[\frac{1 - e^{i(n+2)\pi}}{n+2}\right.$$
$$\left.-\frac{1 - e^{i(n-2)\pi}}{n+2}\right]\frac{n!\, e^{ip_f r_0}}{\left(-ip_f\right)^{n+1}} \quad (16)$$

$$A_3 = \frac{\pi k_e T_{ef}}{2} \sum_{n=-\infty}^{\infty} i^n J_n(p_i z) \left[\pi\omega sin(c_1) + \frac{\pi^2}{2\tau_R} sin\,(c_1)\right] \left[\frac{1 - e^{i(n+2)\pi}}{n+2} - \frac{1 - e^{i(n-2)\pi}}{n+2}\right] \frac{n!\, e^{ip_i r_0}}{(-ip_i)^{n+1}} \tag{17}$$

$$A_4 = -\frac{\pi k_e^2 T_{ef} T_{ei}}{8} r^4 cos2\theta \left[\pi\omega sin(c_1) + \frac{\pi^2}{2\tau_R} sin\,(c_1)\right] \tag{18}$$

Now, substituting the value of A_1, A_2, A_3 and A_4 from EQUATION (15)-(18), respectively, we have:

$$\begin{aligned} S = \frac{A_0}{(2\pi)^3 (2\pi\sigma^2)^{\frac{1}{2}}} & \frac{\pi}{4}\left[\pi\omega \sin(c_1) + \frac{\pi^2}{2\tau_R}\sin(c_1)\right]\left[\frac{1 - e^{i(n+2)\pi}}{n+2} - \frac{1 - e^{i(n-2)\pi}}{n+2}\right]\left[\sum_{n=-\infty}^{\infty} i^n J_n(\Delta p z) \frac{n!\, e^{i\Delta p r_0}}{(-i\Delta p)^{n+1}} - T_{ei} \sum_{n=-\infty}^{\infty} i^n J_n(p_f z) \frac{n!\, e^{ip_f r_0}}{(-ip_f)^{n+1}}\right] \\ & - \frac{\pi^2}{2}\left[\pi\omega \sin(c_1) + \frac{\pi^2}{2\tau_R}\sin(c_1)\right]\left[T_{ef} \sum_{n=-\infty}^{\infty} i^n J_n(p_i z)\left[\frac{1 - e^{i(n+2)\pi}}{n+2} - \frac{1 - e^{i(n-2)\pi}}{n+2}\right] \frac{n!\, e^{ip_i r_0}}{(-ip_i)^{n+1}} + \frac{T_{ef} T_{ei}}{4} r^4 \cos 2\theta\right] \end{aligned} \tag{19}$$

Now, the transitions matrix from EQUATION (19), with the help of S and T, is expressed as

$$\begin{aligned} T = \frac{\pi}{4} & \left[\pi\omega \sin(c_1) + \frac{\pi^2}{2\tau_R}\sin(c_1)\right]\left[\frac{1 - e^{i(n+2)\pi}}{n+2} - \frac{1 - e^{i(n-2)\pi}}{n-2}\right]\left[\sum_{n=-\infty}^{\infty} i^n J_n(\Delta p z) \frac{n!\, e^{i\Delta p r_0}}{(-i\Delta p)^{n+1}} - T_{ei} \sum_{n=-\infty}^{\infty} i^n J_n(p_f z) \frac{n!\, e^{ip_f r_0}}{(-ip_f)^{n+1}}\right] \\ & - \frac{\pi^2}{2}\left[\pi\omega \sin(c_1) + \frac{\pi^2}{2\tau_R}\sin(c_1)\right]\left[T_{ef} \sum_{n=-\infty}^{\infty} i^n J_n(p_i z)\left[\frac{1 - e^{i(n+2)\pi}}{n+2} - \frac{1 - e^{i(n-2)\pi}}{n-2}\right] \frac{n!\, e^{ip_i r_0}}{(-ip_i)^{n+1}} + \frac{T_{ef} T_{ei}}{4} r^4 \cos 2\theta\right] \end{aligned} \tag{20}$$

Now, on substituting the value of T form EQUATION (20), we get DCS with EQUATION (21) as shown below:

$$\frac{d\sigma}{d\Omega} = \frac{k_f}{k_i}|T|^2 \tag{21}$$

In EQUATION (21), k_f represents the final momentum of the positron, k_i denotes the initial momentum of the positron, and T is the transition matrix describing the interaction process. EQUATION (21) is computed by substituting the values from EQUATION (20) using the

MATLAB programming language. The parameter values are taken from various authors: $\omega = 0 - 5\,\text{eV}$, $r = 1\,\text{Å}$, $k_i = 2\,\text{eV}$, $k_f = 1.5\,\text{eV}$, $\theta = 0 - 10°$, $\phi = \pi/2$, $n = 1$, and $z = 0 - 3°/\text{eV}$, with temperature around room temperature as referenced in [21, 11]. The potential sources of error in this work arise from the use of various assumptions and simplifications, including the neglect of certain terms to facilitate analytical derivation and reduce computational complexity. These approximations, while necessary for tractability, may impact the accuracy and completeness of the results, especially under conditions where the neglected factors play a significant role.

RESULTS AND DISCUSSIONS

The DCS with projected positrons on a target (likely an electron target, in a scattering experiment) shown in FIGURE 1 increases with increasing positron energy at low energies, reaches a maximum, and then decreases with further increases in the incidence energy of the positron. This is typical in scattering experiments, as the probability of interaction tends to rise with energy due to increased effective cross-sectional area for scattering. The maximum DCS at around 0.5 eV suggests that at this energy, the interaction between the positron and the target is resonant, which enhances the interaction cross-section.

After the maximum, the DCS decreases with increasing positron energy. This is because at higher energies, the positron moves too fast to interact significantly with the target electrons, and thus the scattering probability (or DCS) decreases. In high-energy scattering, the target cannot easily respond to the fast-moving projectile, leading to less efficient interaction. At very high positron energies, the DCS becomes almost constant. This is due to the fact that the positron's kinetic energy is high enough that its interaction with the target is no longer strongly dependent on the energy of the positron itself. At high energies, the cross section for scattering often approaches a constant value because the projectiles pass through the target without undergoing much deflection. The observation of a peak in the DCS around 0.5 eV at temperatures 300 K and 325 K suggests a resonance effect influenced by the laser field in the system. In the presence of a laser field, the interaction dynamics between the positron and the target could change significantly, especially near resonance energies, because the laser can modify the energy states or induce additional interaction channels.

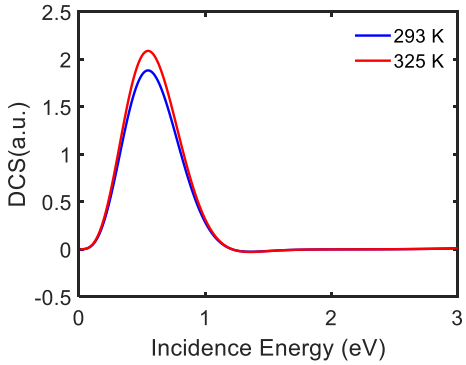

FIGURE 1. DCS with incidence of positron at different temperature

The observation shows that the thermal environment has a high impact on DCS. At the given temperatures (300 K and 325 K), the target (likely an electron) can be thermally excited, affecting its energy distribution. The thermal effect is responsible for the slight shifts or variations in the DCS observed at these temperatures. The temperature has no significant effect on DCS at higher incidence energies. As the positron's energy increases, the thermal energy of the target electrons becomes negligible in comparison. Shorifuddoza et al. studied the scattering of $e^{\mp}$ from ytterbium atoms and found that the DCS decreases with incidence energy and has a similar nature to that shown in FIGURE 1 in the lower energy region [23]. Lozanon et al. also studied electron and positron scattering cross sections from CO_2 and found similar nature as shown in FIGURE 1 [24].

FIGURE 2 shows that as the z-value increases, the DCS decreases and eventually becomes constant. This behavior can be explained by the interaction between the incoming positron and the electrons of the target. As the z-value increases, the target has more electrons, which leads to a stronger Coulombic interaction between the positron and the target. Initially, this enhances the scattering process, but as the z-value becomes very large, the interactions become more tightly bound, and the positron is less likely to undergo significant scattering. Therefore, the DCS decreases and stabilizes as the z-value increases, indicating that at high z-values, the atomic characteristics of the target have less effect on the scattering process. In line with the findings in FIGURE 1, the DCS decreases with increasing positron energy at a fixed scattering angle. This observation is typical in scattering experiments where, at higher energies, the interaction between the positron and the target becomes less significant. At lower energies, the positron is more likely to undergo multiple interactions with the target, leading to a higher scattering cross-section. However, as the positron's energy increases, the projectile moves faster, and the interaction becomes weaker, leading to a decrease in the DCS. This trend mirrors the behavior observed in FIGURE

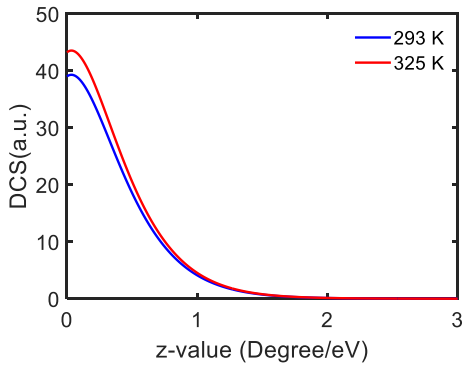

FIGURE 2. DCS with Z-value at different temperature

The DCS decreases with increasing scattering angle at a fixed positron energy. At smaller angles, the projectile tends to scatter in the forward direction, which generally corresponds to a higher probability of interaction. As the scattering angle increases, the interaction probability diminishes, leading to a reduction in the DCS. The findings emphasize that for this particular system, lower energies (below 0.5 eV) are most significant for studying the DCS. Under these conditions, the DCS is higher, which means the interactions between the positron and target

electrons are more likely to result in scattering events. Another key observation from FIGURE 2 is that the DCS at 325 K is higher than at 300 K. This difference can be attributed to the increased oscillatory motion of the target electrons and the positron at the higher temperature. At higher temperatures, the electrons in the target are more thermally excited, which leads to more dynamic interactions with the incoming positron. Additionally, the positron itself may undergo greater oscillations in response to the thermal environment. These enhanced oscillations increase the likelihood of scattering interactions, resulting in a higher DCS at 325 K compared to 300 K. This suggests that temperature plays an important role in enhancing the scattering process by making the particles involved more active.

FIGURE 3 shows that the DCS increases with an increase in the number of laser field photons. This behavior indicates that the laser field plays a significant role in enhancing the scattering process. As the number of photons in the laser field increases, the interaction between the positron and the target electrons also increases. The presence of an external laser field can modify the potential between the incoming particles and the target, leading to more frequent or stronger scattering events. The finding that the DCS is higher at 325 K compared to 300 K further supports the idea that temperature affects the scattering dynamics. At higher temperatures (325 K), the target particles are more thermally excited, which leads to greater motion and increased interaction probability with the positron. This higher thermal excitation results in more effective scattering, leading to a higher DCS. In contrast, at lower temperatures (300 K), the particles are less thermally active, reducing the interaction efficiency and, therefore, the DCS. This temperature-dependent behavior highlights the importance of thermal energy in scattering events and suggests that at higher temperatures, the system exhibits more dynamic scattering interactions.

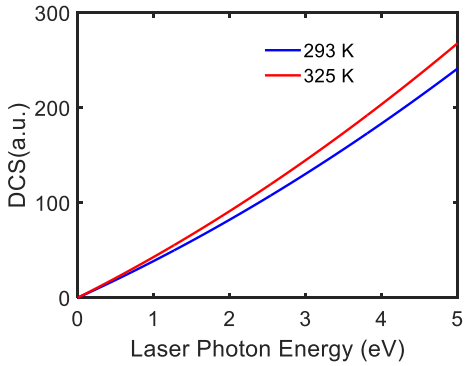

FIGURE 3. DCS with laser field photons at different temperature

FIGURE 4 shows that the DCS decreases as the pulse duration (τ_R) increases. This observation suggests that the interaction between the positron and the target electrons is influenced by the length of the laser pulse. When the pulse duration is shorter, the intensity of the laser field is more concentrated in time, which can lead to a stronger interaction between the positron and the target. As the pulse duration increases, the energy delivery from the laser field becomes spread over a longer time period, reducing the overall effectiveness of the interaction. This reduced interaction likely leads to a decrease in the DCS with increasing pulse duration, as the interaction between the projectile and the target becomes less effective. The finding that the

DCS is higher at 325 K than at 300 K for the same τ_R indicates that temperature plays an important role in modulating the scattering process, particularly in relation to the pulse duration. The temperature dependence suggests that thermal energy contributes to the resonance effect in scattering, and at higher temperatures, the system is more responsive to the laser pulse, leading to a higher DCS.

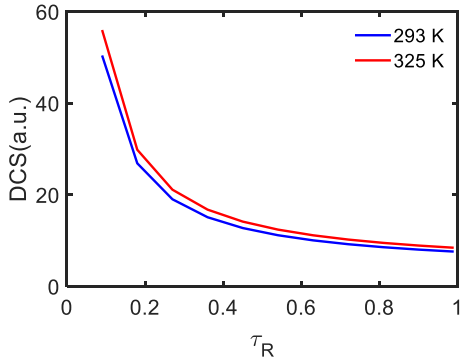

FIGURE 4. DCS with τ_R at different tempearture

Consequently, the DCS becomes constant because the interaction is predominantly governed by the single-photon process, where the positron interacts with only one photon over the extended duration of the pulse. This trend reflects the nature of longer pulse interactions, where the laser field is no longer strong enough to induce multiple-photon scattering events, leading to a reduction in the overall scattering efficiency. The higher DCS at shorter pulse durations can be explained by the fact that shorter pulses cause multiple-photon interactions in the thermal environment. In shorter pulses, the energy from the laser field is delivered more rapidly, which increases the likelihood that the positron will interact with more than one photon during the scattering event. This results in an enhanced scattering process and a higher DCS. The shorter pulse duration creates a more intense field in a brief time, causing a resonance effect that amplifies the interaction between the positron and the target electrons. As a result, the DCS is higher at shorter pulse durations because multiple-photon contribute to the scattering process, leading to an increase in the scattering cross-section.

The limitations of this work include its restriction to the non-relativistic regime, where spin effects are neglected and only the z-component of relevant variables, such as incident energy, temperature, and photon energy, are considered. Other important parameters — such as inter-particle distance, scattering angle, and the phase of the developed equation — were not investigated. Additionally, this study is entirely theoretical, and thus lacks experimental validation, which is essential for assessing its practical applicability. Furthermore, the model does not account for transition states, which limits its ability to accurately calculate the DCS in scenarios involving state transitions.

CONCLUSION

This study comprehensively analyzed the factors influencing the DCS in positron scattering, focusing on key parameters such as positron energy, temperature, z-value, laser field intensity, and pulse duration. The results reveal that the DCS increases with positron energy at low

levels, peaks around 0.5 eV, and then declines with further energy increase, highlighting a resonance-driven interaction. A decrease in DCS with increasing z-value suggests that heavier target atoms reduce scattering efficiency, while higher photon numbers in the laser field enhance DCS, indicating stronger positron-target coupling under laser influence. Additionally, longer pulse durations reduce DCS, as the interaction becomes less effective. Practically, these findings can be applied to optimizing positron-based diagnostic tools in material science, such as defect imaging in semiconductors, and in laser-assisted scattering experiments for precision measurements. It is recommended that future work includes experimental validation and considers spin effects, transition states, and other scattering parameters to develop more comprehensive and realistic models for advanced applications in atomic and condensed matter physics.

ACKNOWLEDGEMENTS

The authors would like to thank all the faculty and non-faculty members of the Department of Physics, Patan Multiple Campus, Patan Dhoka, Lalitpur, Nepal, for providing research facilities and a peaceful environment during this study.

REFERENCES

[1] A. Bhatia, "Scattering and its applications to various atomic processes: Elastic scattering, resonances, photoabsorption, Rydberg states, and opacity of the atmosphere of the Sun and stellar objects," *Atoms*, vol. 8, no. 4, p. 78, 2020.
[2] N. Kroll and K. Watson, "Charged-particles scattering in the presence of a strong electromagnetic wave," *Phys. Rev. A*, vol. 8, pp. 804–809, 1973.
[3] D. J. Griffiths and D. F. Schroeter, *Introduction to Quantum Mechanics*, 3rd ed. Cambridge, U.K.: Cambridge University Press, 2018.
[4] T. Podszus and A. Di Piazza, "First-order strong-field QED processes including the damping of particle states," *Phys. Rev. D*, vol. 104, no. 1, p. 016014, 2021.
[5] L. Rosenberg and F. Zhou, "Generalized Volkov wave functions: Application to laser-assisted scattering," *Phys. Rev. A*, vol. 47, no. 3, p. 2146, 1993.
[6] K. Fedus and G. Karwasz, "Positron scattering at thermal energies," *Acta Phys. Pol. A*, vol. 125, no. 3, pp. 829–832, 2014.
[7] J. T. Mendonca and A. Serbeto, "Volkov solutions for relativistic quantum plasmas," *Phys. Rev. E*, vol. 83, no. 2, p. 026406, 2011.
[8] S. Taj, B. Manaut, and M. El Idrissi, "Laser-assisted positron-impact ionization of hydrogen atoms," *Acta Phys. Pol. A*, vol. 136, no. 1, p. 78, 2019.
[9] P. Fraser, "Positrons and positronium in gases," *Adv. At. Mol. Phys.*, vol. 4, pp. 63–107, 1968.
[10] S. Singh *et al*., "Theoretical formalism to estimate the positron scattering cross section," *J. Phys. Chem. A*, vol. 120, no. 28, pp. 5685–5692, 2016.
[11] J. Larkin *et al*., "Numerical study of positron-hydrogen scattering," *Phys. Rev. A*, vol. 57, no. 4, pp. 2572–2577, 1998. doi: 10.1103/PhysRevA.57.2572.
[12] S. H. Dhobi *et al*., "Differential cross-section in the presence of a weak laser field for inelastic scattering," *Ukr. J. Phys.*, vol. 67, no. 4, pp. 227–235, 2022, doi: 10.15407/ujpe67.4.227.
[13] S. P. Roshchupkin, V. V. Dubov, and D. V. Doroshenko, "Resonance of the annihilation channel of a laser-assisted electron-positron scattering," in *Proc. PhotonIcs Electromagn. Res. Symp. (PIERS-Spring)*, Rome, Italy, Jun. 2019, pp. 4220–4225.
[14] J. Pan, S. M. Li, and J. Berakdar, "Laser-assisted positron-impact ionization of atomic hydrogen," *Opt. Lett.*, vol. 32, no. 6, pp. 585–587, 2007.

[15] W. Y. Du, B. H. Wang, and S. M. Li, "Nonlinear effects in the laser-assisted scattering of a positron by a muon," *Mod. Phys. Lett. B*, vol. 32, no. 05, p. 1850058, 2018.
[16] K. A. Bornikov, I. P. Volobuev, and Y. V. Popov, "On Compton ionization of positronium by twisted photons," *Moscow Univ. Phys. Bull.*, vol. 80, no. 1, pp. 76–84, 2025.
[17] Z. K. Dou *et al*., "Compact spin-polarized positron acceleration in multilayer microhole-array films," *Phys. Rev. E*, vol. 111, no. 3, p. 035209, 2025.
[18] Q. Su and J. H. Eberly, "Model atom for multiphoton physics," *Phys. Rev. A*, vol. 44, no. 9, pp. 5997–6008, 1991. doi: 10.1103/PhysRevA.44.5997.
[19] F. He, A. Becker, and U. Thumm, "Strong-field modulated diffraction effects in the correlated electron-nuclear motion in dissociating H_2^+," *Phys. Rev. Lett.,* vol. 101, no. 21, p. 213002, 2008.
[20] X. H. Ji *et al*., "Quantum dynamics of positron-hydrogen scattering and three-body bound state formation with an assisting laser field," *J. Phys. B: At. Mol. Opt. Phys.*, vol. 57, no. 1, p. 015203, 2024.
[21] S. H. Dhobi *et al*., "Differential cross section with Volkov-thermal wave function in Coulomb potential," *Atom Indonesia*, vol. 50, no. 1, pp. 19–25, 2024.
[22] S. H. Dhobi *et al*., "Study of thermodynamics of a thermal electron in scattering," *Heliyon*, vol. 8, no. 12, 2022.
[23] M. Shorifuddoza *et al*., "Scattering of $e^{\mp}$ from ytterbium atoms," *Eur. Phys. J. D*, vol. 73, pp. 1–23, 2019.
[24] A. I. Lozano *et al*., "Electron and positron scattering cross sections from CO_2: A comparative study over a broad energy range (0.1–5000 eV)," *J. Phys. Chem. A*, vol. 126, no. 36, pp. 6032–6046, 2022.